Collision-geometry fluctuations and triangular flow in heavy-ion collisions

B. Alver and G. Roland

Laboratory for Nuclear Science, Massachusetts Institute of Technology, Cambridge, Massachusetts 02139-4307, USA
(Received 28 February 2010; published 21 May 2010)

We introduce the concepts of participant triangularity and triangular flow in heavy-ion collisions, analogous to the definitions of participant eccentricity and elliptic flow. The participant triangularity characterizes the triangular anisotropy of the initial nuclear overlap geometry and arises from event-by-event fluctuations in the participant-nucleon collision points. In studies using a multiphase transport model (AMPT), a triangular flow signal is observed that is proportional to the participant triangularity and corresponds to a large third Fourier coefficient in two-particle azimuthal correlation functions. Using two-particle azimuthal correlations at large pseudorapidity separations measured by the PHOBOS and STAR experiments, we show that this Fourier component is also present in data. Ratios of the second and third Fourier coefficients in data exhibit similar trends as a function of centrality and transverse momentum as in AMPT calculations. These findings suggest a significant contribution of triangular flow to the ridge and broad away-side features observed in data. Triangular flow provides a new handle on the initial collision geometry and collective expansion dynamics in heavy-ion collisions.

I. INTRODUCTION

Studies of two-particle azimuthal correlations have become a key tool in characterizing the evolution of the strongly interacting medium formed in ultrarelativistic nucleus-nucleus collisions. Traditionally, the observed two-particle azimuthal correlation structures are thought to arise from two distinct contributions. The dominant one is the "elliptic flow" term, related to anisotropic hydrodynamic expansion of the medium from an anisotropic initial state [1–9]. In addition, one observes so-called "nonflow" contributions from, e.g., resonances and jets, which may be modified by their interactions with the medium [10–12].

The strength of anisotropic flow is usually quantified with a Fourier decomposition of the azimuthal distribution of observed particles relative to the reaction plane [13]. The experimental observable related to elliptic flow is the second Fourier coefficient, "v_2." The elliptic flow signal has been studied extensively in Au + Au collisions at the Relativistic Heavy Ion Collider (RHIC) as a function of pseudorapidity, centrality, transverse momentum, particle species and center-of-mass energy [3–7]. The centrality and transverse momentum dependence of v_2 has been found to be well described by hydrodynamic calculations, which for a given equation of state, can be used to relate a given initial energy density distribution to final momentum distribution of produced particles [14]. In these calculations, the v_2 signal is found to be proportional to the eccentricity, ε_2, of the initial collision region defined by the overlap of the colliding nuclei [15]. Detailed comparisons of the observed elliptic flow effects with hydrodynamic calculations have led to the conclusion that a new state of strongly interacting matter with very low shear viscosity, compared to its entropy density, has been created in these collisions [14,16–18].

Measurements of nonflow correlations in heavy-ion collisions, in comparison to corresponding studies in $p + p$ collisions, provide information on particle production mechanisms [19] and parton-medium interactions [10–12]. Different methods have been developed to account for the contribution of elliptic flow to two-particle correlations in these studies of the underlying nonflow correlations [10,19–22]. The most commonly used approach is the zero yield at minimum method (ZYAM), where one assumes that the associated particle yield correlated with the trigger particle is zero at the minimum as a function of $\Delta\phi$ after elliptic flow contribution is taken out [21]. The ZYAM approach has yielded rich correlation structures at $\Delta\phi \approx 0°$ and $\Delta\phi \approx 120°$ for different p_T ranges [23–26]. These structures, which are not observed in $p + p$ collisions at the same collision energy, have been referred to as the "ridge" and "broad away-side" or "shoulder." The same correlation structures have been found to be present in Pb + Au collisions at $\sqrt{s_{NN}} = 17.4$ GeV at the SPS [27]. Measurements at RHIC have shown that these structures extend out to large pseudorapidity separations of $\Delta\eta > 2$, similar to elliptic flow correlations [25]. The ridge and broad away-side structures have been extensively studied experimentally [12,23–26,28] and various theoretical models have been proposed to understand their origin [29–36]. A recent review of the theoretical and experimental results can be found in Ref. [37].

In this article, we propose that the observed ridge and broad away-side features in two-particle correlations may be due to an average triangular anisotropy in the initial collision geometry which is caused by event-by-event fluctuations and which leads to a triangular anisotropy in azimuthal particle production through the collective expansion of the medium. It was shown that, in the NEXSPHERIO hydrodynamic model, ridge and broad away-side structures in two particle correlations arise if nonsmooth initial conditions are introduced [36]. Sorensen has suggested that fluctuations of the initial collision geometry may lead to higher-order Fourier components in the azimuthal correlation function through collective effects [38]. An analysis of higher-order components in the Fourier decomposition of azimuthal particle distributions, including

the odd terms, was proposed by Mishra *et al.* to probe superhorizon fluctuations in the thermalization stage [39]. In this work, we show that the second and third Fourier components of two-particle correlations may be best studied by treating the components of corresponding initial geometry fluctuations on equal footing. To reduce contributions of nonflow correlations, which are most prominent in short pseudorapidity separations, we focus on azimuthal correlations at long ranges in pseudorapidity. We show that the ridge and broad away-side structures can be well described by the first three coefficients of a Fourier expansion of the azimuthal correlation function

$$\frac{dN^{\text{pairs}}}{d\Delta\phi} = \frac{N^{\text{pairs}}}{2\pi}\left[1 + \sum_n 2\mathbf{V}_{n\Delta}\cos(n\Delta\phi)\right], \qquad (1)$$

where the first component, $\mathbf{V}_{1\Delta}$[1], is understood to be due to momentum conservation and directed flow and the second component $\mathbf{V}_{2\Delta}$ is dominated by the contribution from elliptic flow. Studies in a multiphase transport model (AMPT) [40] suggest that not only the elliptic flow term, $\mathbf{V}_{2\Delta}$, but also a large part of the correlations measured by the $\mathbf{V}_{3\Delta}$ term, arises from the hydrodynamic expansion of the medium.

II. FOURIER DECOMPOSITION OF AZIMUTHAL CORRELATIONS

In the existing correlation data, different correlation measures such as $R(\Delta\eta, \Delta\phi)$ [19], $N\hat{r}(\Delta\eta, \Delta\phi)$ [41], and $1/N_{\text{trig}}dN/d\Delta\phi(\Delta\eta, \Delta\phi)$ [25] have been used to study different sources of particle correlations. The azimuthal projection of all of these correlation functions have the form

$$C(\Delta\phi) = A\frac{dN^{\text{pairs}}}{d\Delta\phi} + B, \qquad (2)$$

where the scale factor A and offset B depend on the definition of the correlation function as well as the pseudorapidity range

---

[1]Note the distinction between $\mathbf{V}_{n\Delta}$ and v_n. See Eqs. (10) and (11) for details.

of the projection [25]. Examples of long range azimuthal correlation distributions are shown in Fig. 1 for inclusive correlations from PHOBOS and STAR [19,41] and high-p_T triggered correlations from PHOBOS [25] for mid-central Au + Au collisions obtained by projecting the two-dimensional correlation functions onto the $\Delta\phi$ axis at pseudorapidity separations of $1.2 < \Delta\eta < 1.9$ for STAR data and $2 < \Delta\eta < 4$ for PHOBOS data. The correlation function data used in this study are available at Refs. [42–44]. Also shown in Fig. 1 are the first three Fourier components of the azimuthal correlations and the residual after these components are taken out. The data is found to be very well described by the three Fourier components.

III. PARTICIPANT TRIANGULARITY AND TRIANGULAR FLOW

It is useful to recall that traditional hydrodynamic calculations start from a smooth matter distribution given by the transverse overlap of two Woods-Saxon distributions. In such calculations, elliptic flow is aligned with the orientation of the reaction plane defined by the impact parameter direction and the beam axis and by symmetry, no $\mathbf{V}_{3\Delta}$ component arises in the azimuthal correlation function. To describe this component in terms of hydrodynamic flow requires a revised understanding of the initial collision geometry, taking into account fluctuations in the nucleon-nucleon collision points from event to event. The possible influence of initial geometry fluctuations was used to explain the surprisingly large values of elliptic flow measured for central Cu + Cu collision, where the average eccentricity calculated with respect to the reaction plane angle is small [8]. For a Glauber Monte Carlo event, the minor axis of eccentricity of the region defined by nucleon-nucleon interaction points does not necessarily point along the reaction plane vector but may be tilted. The "participant eccentricity" [8,45] calculated with respect to this tilted axis is found to be finite even for most central events and significantly larger than the reaction plane eccentricity for the smaller Cu + Cu system. Following this idea, event-by-event elliptic flow fluctuations have been measured and found to be
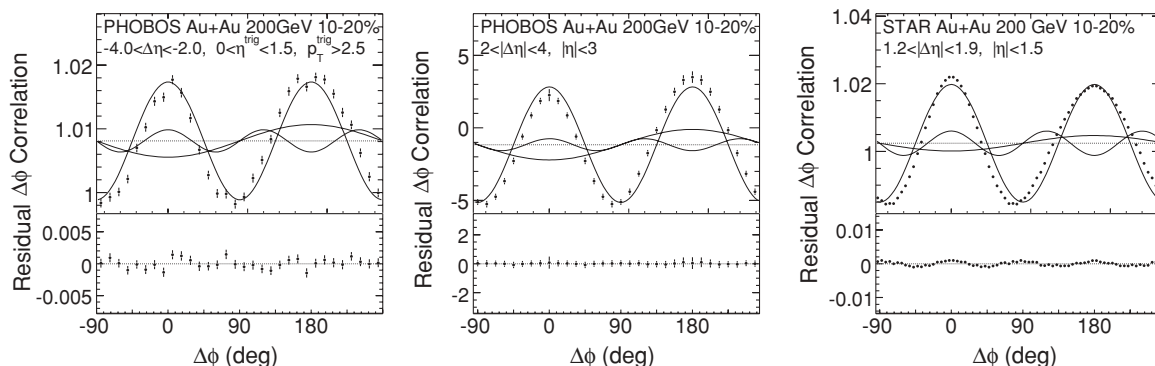

FIG. 1. (Top) Azimuthal correlation functions for mid-central (10–20%) Au + Au collisions at $\sqrt{s_{NN}} = 200$ GeV obtained from projections of two-dimensional $\Delta\eta$, $\Delta\phi$ correlation measurements by PHOBOS [19,25] and STAR [41]. The transverse momentum and pseudorapidity ranges are indicated on the figures. Errors bars are combined systematic and statistical errors. The first three Fourier components are shown in solid lines. (Bottom) The residual correlation functions after the first three Fourier components are subtracted.
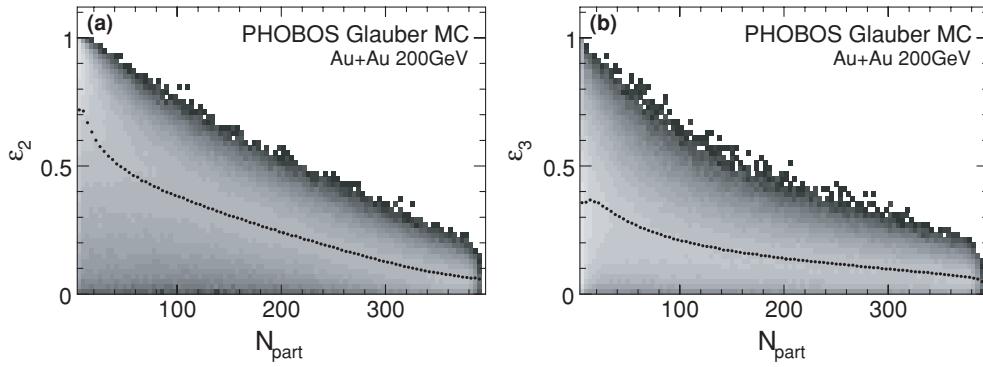
FIG. 2. Distribution of (a) eccentricity, ε_2, and (b) triangularity, ε_3, as a function of number of participating nucleons, N_{part}, in $\sqrt{s_{NN}} = 200$ GeV Au + Au collisions.

consistent with the expected fluctuations in the initial state geometry with the new definition of eccentricity [46]. In this article, we use this method of quantifying the initial anisotropy exclusively.

Mathematically, the participant eccentricity is given as

$$\varepsilon_2 = \frac{\sqrt{(\sigma_y^2 - \sigma_x^2)^2 + 4(\sigma_{xy})^2}}{\sigma_y^2 + \sigma_x^2}, \tag{3}$$

where σ_x^2, σ_y^2, and σ_{xy}, are the event-by-event (co-)variances of the participant nucleon distributions along the transverse directions x and y [8]. If the coordinate system is shifted to the center of mass of the participating nucleons such that $\langle x \rangle = \langle y \rangle = 0$, it can be shown that the definition of eccentricity is equivalent to

$$\varepsilon_2 = \frac{\sqrt{\langle r^2 \cos(2\phi_{\text{part}}) \rangle^2 + \langle r^2 \sin(2\phi_{\text{part}}) \rangle^2}}{\langle r^2 \rangle} \tag{4}$$

in this shifted frame, where r and ϕ_{part} are the polar coordinate positions of participating nucleons. The minor axis of the ellipse defined by this region is given as

$$\psi_2 = \frac{\text{atan2}(\langle r^2 \sin(2\phi_{\text{part}}) \rangle, \langle r^2 \cos(2\phi_{\text{part}}) \rangle) + \pi}{2}. \tag{5}$$

Since the pressure gradients are largest along ψ_2, the collective flow is expected to be the strongest in this direction. The definition of v_2 has conceptually changed to refer to the second Fourier coefficient of particle distribution with respect to ψ_2 rather than the reaction plane

$$v_2 = \langle \cos(2(\phi - \psi_2)) \rangle. \tag{6}$$

This change has not affected the experimental definition since the directions of the reaction plane angle or ψ_2 are not *a priori* known.

Drawing an analogy to eccentricity and elliptic flow, the initial and final triangular anisotropies can be quantified as participant triangularity, ε_3, and triangular flow, v_3, respectively:

$$\varepsilon_3 \equiv \frac{\sqrt{\langle r^2 \cos(3\phi_{\text{part}}) \rangle^2 + \langle r^2 \sin(3\phi_{\text{part}}) \rangle^2}}{\langle r^2 \rangle} \tag{7}$$

$$v_3 \equiv \langle \cos(3(\phi - \psi_3)) \rangle, \tag{8}$$

where ψ_3 is the minor axis of participant triangularity given by

$$\psi_3 = \frac{\text{atan2}(\langle r^2 \sin(3\phi_{\text{part}}) \rangle, \langle r^2 \cos(3\phi_{\text{part}}) \rangle) + \pi}{3}. \tag{9}$$

It is important to note that the minor axis of triangularity is found to be uncorrelated with the reaction plane angle and the minor axis of eccentricity in Glauber Monte Carlo calculations. This implies that the average triangularity calculated with respect to the reaction plane angle or ψ_2 is zero. The participant triangularity defined in Eq. (7), however, is calculated with respect to ψ_3 and is always finite.

The distributions of eccentricity and triangularity calculated with the PHOBOS Glauber Monte Carlo implementation [47] for Au + Au events at $\sqrt{s_{NN}} = 200$ GeV are shown in Fig. 2. The value of triangularity is observed to fluctuate event by event and have an average magnitude of the same order as eccentricity. Transverse distribution of nucleons for a sample Monte Carlo event with a high value of triangularity is shown in Fig. 3. A clear triangular anisotropy can be seen in the region defined by the participating nucleons.
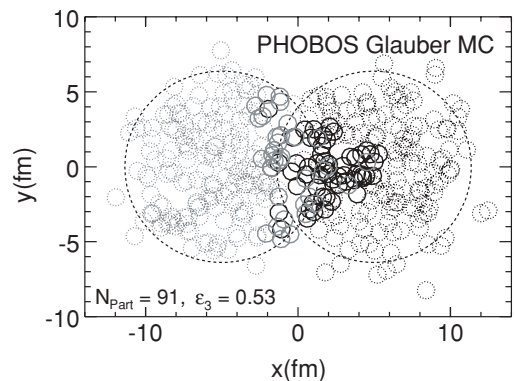

FIG. 3. Distribution of nucleons on the transverse plane for a $\sqrt{s_{NN}} = 200$ GeV Au + Au collision event with $\varepsilon_3 = 0.53$ from Glauber Monte Carlo. The nucleons in the two nuclei are shown in gray and black. Wounded nucleons (participants) are indicated as solid circles, while spectators are dotted circles.
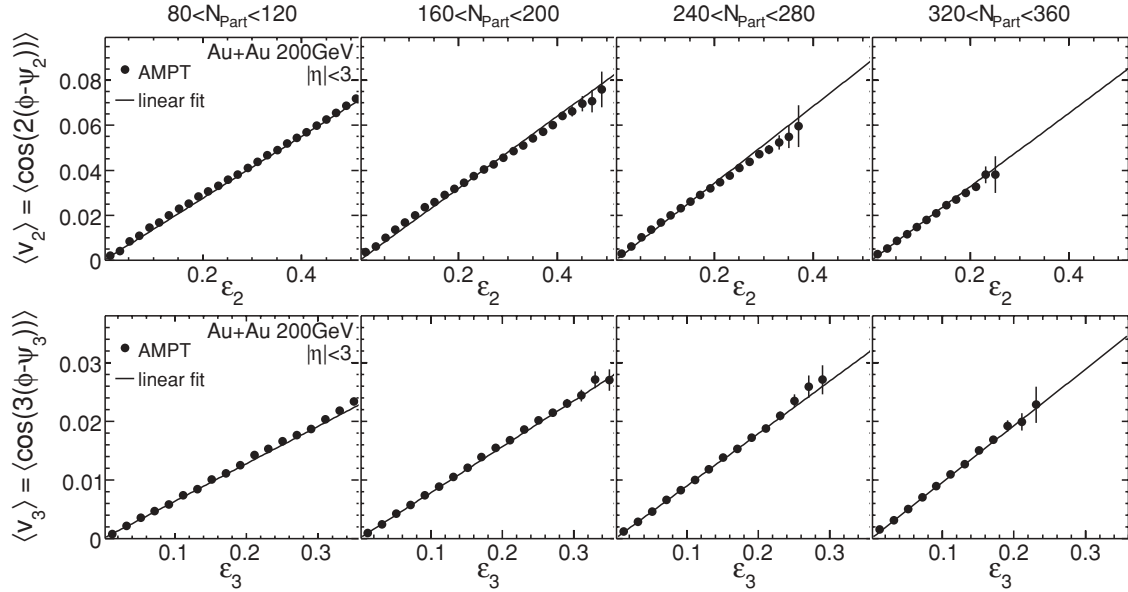
FIG. 4. (Top) Average elliptic flow, $\langle v_2 \rangle$, as a function of eccentricity, ε_2; (bottom) average triangular flow, $\langle v_3 \rangle$, as a function of triangularity, ε_3, in $\sqrt{s_{NN}} = 200$ GeV Au + Au collisions from the AMPT model in bins of number of participating nucleons. Error bars indicate statistical errors. A linear fit to the data is shown.

IV. TRIANGULAR FLOW IN THE AMPT MODEL

To assess the connection between triangularity and the ridge and broad away-side features in two-particle correlations, we study elliptic and triangular flow in the AMPT model. AMPT is a hybrid model which consists of four main components: initial conditions, parton cascade, string fragmentation, and a relativistic transport model for hadrons. The model successfully describes main features of the dependence of elliptic flow on centrality and transverse momentum [40]. Ridge and broad away-side features in two-particle correlations are also observed in the AMPT model [48,49]. Furthermore, the dependence of quantitative observables such as away-side rms width and away-side splitting parameter D on transverse momentum and reaction plane in AMPT reproduces the experimental results successfully, where a ZYAM-based elliptic flow subtraction is applied to both the data and the model [50,51].

The initial conditions of AMPT are obtained from Heavy Ion Jet Interaction Generator (HIJING) [52]. HIJING uses a Glauber Model implementation that is similar to the PHOBOS implementation to determine positions of participating nucleons. It is possible to calculate the values of ε_2, ψ_2, ε_3, and ψ_3 event by event from the positions of these nucleons [see Eqs. (4), (5), (7), and (9)]. Next, we calculate the magnitudes of elliptic and triangular flow with respect to ψ_2 and ψ_3 respectively as defined in Eqs. (6) and (8).

The average value of elliptic flow, v_2, and triangular flow, v_3, for particles in the pseudorapidity range $|\eta| < 3$ in $\sqrt{s_{NN}} = 200$ GeV Au + Au collisions from AMPT are shown as a function of ε_2 and ε_3 in Fig. 4 for different ranges of number of participating nucleons. As previously expected, the magnitude of v_2 is found to be proportional to ε_2. We observe that a similar linear relation is also present between triangular flow and triangularity.

After establishing that triangular anisotropy in initial collision geometry leads to a triangular anisotropy in particle production, we investigate the contribution of triangular flow to the observed ridge and broad away-side features in two-particle azimuthal correlations. For a given pseudorapidity window, the Fourier coefficients of two-particle azimuthal correlations, $\mathbf{V}_{n\Delta}$, can be calculated in AMPT by averaging $\cos(n\Delta\phi)$ over all particle pairs. Contributions from elliptic (triangular) flow is present in the second (third) Fourier coefficient of $\Delta\phi$ distribution since

$$\int \frac{1}{4\pi^2} \{1 + 2v_n \cos(n\phi)\}\{1 + 2v_n \cos(n(\phi + \Delta\phi))\} d\phi$$
$$= \frac{1}{2\pi} \{1 + 2v_n^2 \cos(n\Delta\phi)\}. \quad (10)$$

For a given pseudorapidity window, this contribution can be calculated from average elliptic (triangular) flow values as

$$\mathbf{V}_{n\Delta}^{\text{flow}} = \frac{\langle \varepsilon_n^2 \rangle}{\langle \varepsilon_n \rangle^2} \frac{\int \frac{dN}{d\eta}(\eta_1)\frac{dN}{d\eta}(\eta_2)\langle v_n(\eta_1)\rangle\langle v_n(\eta_2)\rangle d\eta_1 d\eta_2}{\int \frac{dN}{d\eta}(\eta_1)\frac{dN}{d\eta}(\eta_2)d\eta_1 d\eta_2},$$
$$(11)$$

where $n = 2$ ($n = 3$) and the integration is over the pseudorapidity range of particle pairs. The average single-particle distribution coefficients, $\langle v_n(\eta)\rangle$, are used in this calculation to avoid contributions from nonflow correlations which may be present if the two-particle distributions, $v_n(\eta_1) \times v_n(\eta_2)$, are calculated event by event. The ratio $\langle \varepsilon_n^2 \rangle/\langle \varepsilon_n \rangle^2$ accounts for the difference between $\langle v_n(\eta_1) \times v_n(\eta_2) \rangle$ and $\langle v_n(\eta_1)\rangle \times \langle v_n(\eta_2)\rangle$ expected from initial geometry fluctuations.

We have calculated the magnitude of the second and third Fourier components of two-particle azimuthal correlations and expected contributions to these components from elliptic and triangular flow for particle pairs in $\sqrt{s_{NN}} = 200$ GeV
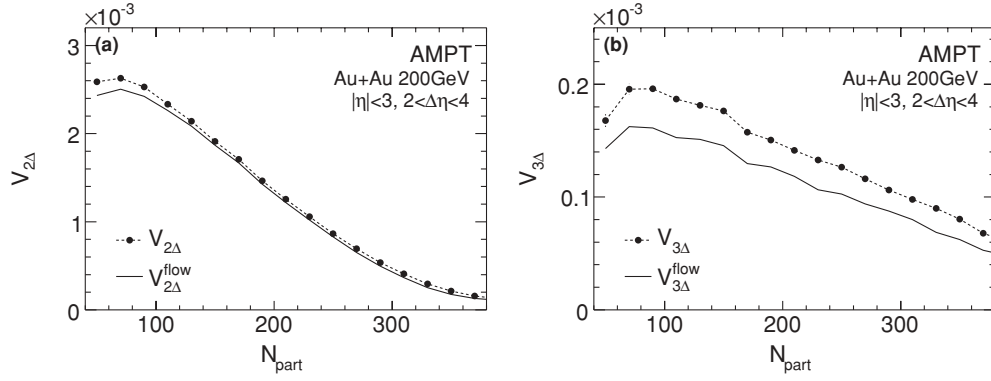
FIG. 5. Dashed lines show (a) second Fourier coefficient, $\mathbf{V}_{2\Delta}$, and (b) third Fourier coefficient, $\mathbf{V}_{3\Delta}$, of azimuthal correlations as a function of number of participating nucleons, N_{part}, in $\sqrt{s_{NN}} = 200$ GeV Au + Au collisions from the AMPT model. Solid lines show the contribution to these coefficients from flow calculated with respect to the minor axis of (a) eccentricity and (b) triangularity.

Au + Au collisions from AMPT within the pseudorapidity range $|\eta| < 3$ and $2 < \Delta\eta < 4$. The results are presented in Fig. 5 as a function of number of participating nucleons. More than 80% of the third Fourier coefficient of azimuthal correlations can be accounted for by triangular flow with respect to the minor axis of triangularity. The difference between $\mathbf{V}_{3\Delta}$ and $\mathbf{V}_{3\Delta}^{\text{flow}}$ may be due to two different effects. There might be contributions from correlations other than triangular flow to $\mathbf{V}_{3\Delta}$ or the angle with respect to which the global triangular anisotropy develops might not be given precisely by the minor axis of triangularity calculated from positions of participant nucleons, i.e., $v_3 = \langle(\cos(3(\phi - \psi_3))\rangle$ might be an underestimate for the magnitude of triangular flow. More detailed studies are needed to distinguish between these two effects.

We have also studied the magnitudes of elliptic and triangular flow more differentially as a function of transverse momentum and number of participating nucleons in the AMPT model. Figure 6 shows the results as a function of transverse momentum for particles at mid-rapidity ($|\eta| < 1$) for different ranges of number of participating nucleons. The dependence of triangular flow on transverse momentum is observed to show similar gross features as elliptic flow. A more detailed comparison can be made by taking the ratio of triangular to elliptic flow, shown in Fig. 7 as a function of number

of participating nucleons for different ranges of transverse momentum. The relative strength of triangular flow is observed to increase with centrality and transverse momentum. This observation is qualitatively consistent with the trends in experimentally measured ridge yield [25].

V. TRIANGULAR FLOW IN EXPERIMENTAL DATA

While AMPT reproduces the expected proportionality of v_2 and ε_2, the absolute magnitude of v_2 is underestimated compared to data and hydrodynamic calculations. To allow a comparison of the $\mathbf{V}_{3\Delta}$ calculations to data, we therefore use the ratio of the third and second Fourier coefficients. For data, this ratio is given by

$$\frac{\mathbf{V}_{3\Delta}}{\mathbf{V}_{2\Delta}} = \frac{\int C(\Delta\phi)\cos(3\Delta\phi)d\Delta\phi}{\int C(\Delta\phi)\cos(2\Delta\phi)d\Delta\phi}. \tag{12}$$

The factors A and B in Eq. (2) cancel out in this ratio. Results for PHOBOS [19,25] and STAR [41] measurements are plotted as a function of number of participating nucleons in Figs. 8(a) and 8(b), respectively. It is observed that $\mathbf{V}_{3\Delta}/\mathbf{V}_{2\Delta}$ increases with centrality and with the transverse momentum of the trigger particle. Comparing inclusive correlations from STAR and PHOBOS, it is also observed that the value of $\mathbf{V}_{3\Delta}/\mathbf{V}_{2\Delta}$
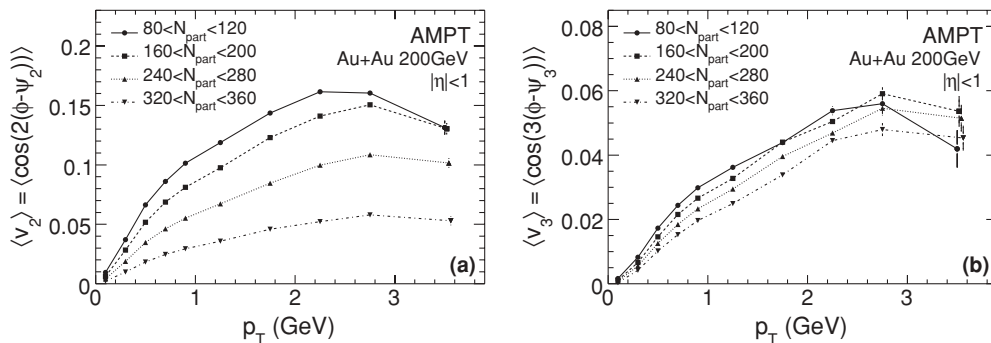

FIG. 6. (a) Elliptic flow, v_2, and (b) triangular flow, v_3, as a function of transverse momentum, p_T, in bins of number of participating nucleons, N_{part}, for particles at midrapidity ($|\eta| < 1$) in $\sqrt{s_{NN}} = 200$ GeV Au + Au collisions from the AMPT model. Error bars indicate statistical errors.
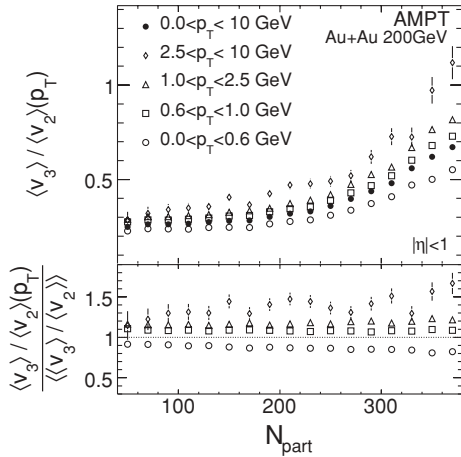
FIG. 7. (Top) the ratio of triangular flow to elliptic flow, $\langle v_3 \rangle / \langle v_2 \rangle$, as a function of number of participating nucleons, N_{part}, for particles at midrapidity ($|\eta| < 1$) in $\sqrt{s_{NN}} = 200$ GeV Au + Au collisions from the AMPT model. Open points show different transverse momentum bins and the filled points show the average over all transverse momentum bins. (Bottom) the ratio of different p_T bins to the average value. Error bars indicate statistical errors.

is higher for STAR measurements. We have found that the ratio $\mathbf{V}_{3\Delta}/\mathbf{V}_{2\Delta}$ calculated for the same PHOBOS measurement in the range $1.2 < |\Delta\eta| < 2$ is consistent with the values for $2 < |\Delta\eta| < 4$ within the systematic uncertainties. The difference between the STAR and PHOBOS measurements is, therefore, likely caused by the difference in pseudorapidity acceptance and the lower transverse momentum reach of the PHOBOS detector compared to STAR.

Also shown in Fig. 8 is the magnitude of $\mathbf{V}_{3\Delta}/\mathbf{V}_{2\Delta}$ in the AMPT model with similar η, $\Delta\eta$, and p_T selections to the available experimental data. The calculations from the model show a qualitative agreement with the data in term of the dependence of $\mathbf{V}_{3\Delta}/\mathbf{V}_{2\Delta}$ on the pseudorapidity region, trigger particle momentum, and centrality. Since the $\mathbf{V}_{3\Delta}$ component of two-particle correlations in the model is known to be mostly due to the triangular anisotropy in the initial collision geometry, this observation suggests that triangular flow may

play an important role in understanding the ridge and broad away-side structures in data.

A closer look at the properties of the ridge and broad away-side is possible via studies of three particle correlations. Triangular flow predicts a very distinct signature in three particle correlation measurements. Two recent publications by the STAR experiment present results on correlations in $\Delta\phi_1$-$\Delta\phi_2$ space for $|\eta| < 1$ [28] and in $\Delta\eta_1$-$\Delta\eta_2$ space for $|\Delta\phi| < 0.7$ [53]. In $\Delta\phi_1$-$\Delta\phi_2$ space, off diagonal away-side correlations have been observed (e.g., first associated particle at $\Delta\phi_1 \approx 120°$ and second associated particle at $\Delta\phi_2 \approx -120°$) consistent with expectations from triangular flow. In $\Delta\eta_1$-$\Delta\eta_2$ space, no correlation structure between the two associated ridge particles was detected, also consistent with triangular flow.

VI. SUMMARY

We have introduced the concepts of participant triangularity and triangular flow, which quantify the triangular anisotropy in the initial and final states of heavy-ion collisions. It has been shown that inclusive and triggered two-particle azimuthal correlations at large $\Delta\eta$ in heavy-ion collisions are well described by the first three Fourier components. It has been demonstrated that event-by-event fluctuations lead to a finite triangularity value in Glauber Monte Carlo events and that this triangular anisotropy in the initial geometry leads to a triangular anisotropy in particle production in the AMPT model. The third Fourier coefficient of azimuthal correlations at large pseudorapidity separations have been found to be dominated by triangular flow in the model. We have studied the ratio of the third and second Fourier coefficients of azimuthal correlations in experimental data and the AMPT model as a function of centrality, pseudorapidity range and trigger particle momentum. A qualitative agreement between data and model has been observed. This suggests that the ridge and broad away-side features observed in two-particle correlation measurements in Au + Au collisions contain a significant, and perhaps dominant, contribution from triangular flow. Our findings support previous evidence from
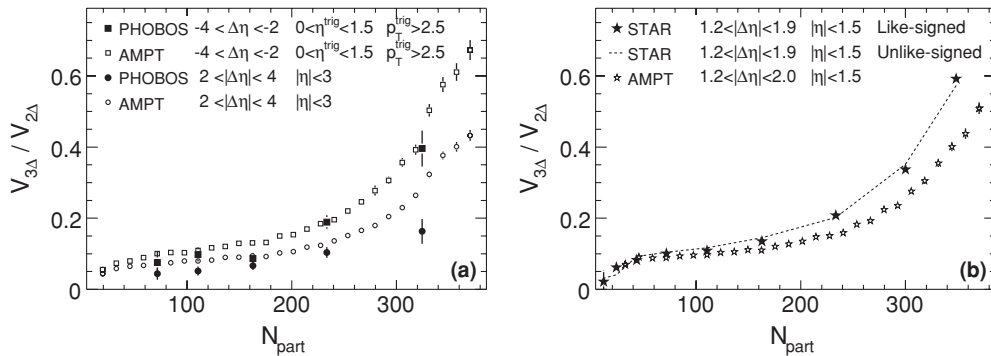

FIG. 8. The ratio of the third to second Fourier coefficients of azimuthal correlations, $\mathbf{V}_{3\Delta}/\mathbf{V}_{2\Delta}$, as a function of number of participating nucleons, N_{part}, for Au + Au collisions at $\sqrt{s_{NN}} = 200$ GeV. Filled points show values derived from (a) PHOBOS [19,25] and (b) STAR [41] data. Pseudorapidity and trigger particle transverse momentum ranges and charge selection of particle pairs for different measurements are indicated on the figures. Open points show results from the AMPT model for similar selection of pseudorapidity and transverse momentum to the available data. Error bars indicate statistical errors for AMPT and combined statistical and systematic errors for the experimental data.

measurements of the system size dependence of elliptic flow and elliptic flow fluctuations on the importance of geometric fluctuations in the initial collision region. Detailed studies of triangular flow can shed new light on the initial conditions and the collective expansion of the matter created in heavy-ion collisions.

[1] K. H. Ackermann *et al.* (STAR Collaboration), Phys. Rev. Lett. **86**, 402 (2001).

[2] K. Adcox *et al.* (PHENIX Collaboration), Phys. Rev. Lett. **89**, 212301 (2002).

[3] S. S. Adler *et al.* (PHENIX Collaboration), Phys. Rev. Lett. **91**, 182301 (2003).

[4] J. Adams *et al.* (STAR Collaboration), Phys. Rev. Lett. **92**, 052302 (2004).

[5] J. Adams *et al.* (STAR Collaboration), Phys. Rev. C **72**, 014904 (2005).

[6] B. B. Back *et al.* (PHOBOS Collaboration), Phys. Rev. Lett. **94**, 122303 (2005).

[7] B. B. Back *et al.* (PHOBOS Collaboration), Phys. Rev. C **72**, 051901 (2005).

[8] B. Alver *et al.* (PHOBOS Collaboration), Phys. Rev. Lett. **98**, 242302 (2007).

[9] A. Adare *et al.* (PHENIX Collaboration), Phys. Rev. Lett. **98**, 162301 (2007).

[10] C. Adler *et al.* (STAR Collaboration), Phys. Rev. Lett. **90**, 082302 (2003).

[11] J. Adams *et al.* (STAR Collaboration), Phys. Rev. Lett. **97**, 162301 (2006).

[12] A. Adare *et al.* (PHENIX Collaboration), Phys. Rev. C **78**, 014901 (2008).

[13] S. Voloshin and Y. Zhang, Z. Phys. C **70**, 665 (1996).

[14] P. F. Kolb, P. Huovinen, U. W. Heinz, and H. Heiselberg, Phys. Lett. B **500**, 232 (2001).

[15] J.-Y. Ollitrault, Phys. Rev. D **46**, 229 (1992).

[16] K. Adcox *et al.* (PHENIX Collaboration), Nucl. Phys. A **757**, 184 (2005).

[17] B. B. Back *et al.* (PHOBOS Collaboration), Nucl. Phys. A **757**, 28 (2005).

[18] J. Adams *et al.* (STAR Collaboration), Nucl. Phys. A **757**, 102 (2005).

[19] B. Alver *et al.* (PHOBOS Collaboration), Phys. Rev. C **81**, 024904 (2010).

[20] J. Adams *et al.* (STAR Collaboration), Phys. Rev. C **73**, 064907 (2006).

[21] N. N. Ajitanand *et al.*, Phys. Rev. C **72**, 011902(R) (2005).

[22] T. A. Trainor and D. T. Kettler, Int. J. Mod. Phys. E **17**, 1219 (2008).

[23] J. Adams *et al.* (STAR Collaboration), Phys. Rev. Lett. **95**, 152301 (2005).

[24] A. Adare *et al.* (PHENIX Collaboration), Phys. Rev. C **77**, 011901 (2008).

[25] B. Alver *et al.* (PHOBOS Collaboration), Phys. Rev. Lett. **104**, 062301 (2010).

[26] B. I. Abelev *et al.* (STAR Collaboration), Phys. Rev. C **80**, 064912 (2009).

[27] D. Adamova *et al.* (CERES Collaboration), Phys. Lett. B **678**, 259 (2009).

[28] B. I. Abelev *et al.* (STAR Collaboration), Phys. Rev. Lett. **102**, 052302 (2009).

[29] C.-Y. Wong, Phys. Rev. C **78**, 064905 (2008).

[30] V. S. Pantuev, arXiv:0710.1882v1 (2007).

[31] S. Gavin, L. McLerran, and G. Moschelli, Phys. Rev. C **79**, 051902(R) (2009).

[32] A. Dumitru, F. Gelis, L. McLerran, and R. Venugopalan, Nucl. Phys. A **810**, 91 (2008).

[33] J. Ruppert and T. Renk, Acta Phys. Pol. Supp. **1**, 633 (2008).

[34] C. A. Pruneau, S. Gavin, and S. A. Voloshin, Nucl. Phys. A **802**, 107 (2008).

[35] R. C. Hwa, arXiv:0904.2159v1 (2009).

[36] J. Takahashi *et al.*, Phys. Rev. Lett. **103**, 242301 (2009).

[37] J. L. Nagle, Nucl. Phys. A **830**, 147c (2009).

[38] P. Sorensen, arXiv:1002.4878v2 (2010).

[39] A. P. Mishra, R. K. Mohapatra, P. S. Saumia, and A. M. Srivastava, Phys. Rev. C **77**, 064902 (2008).

[40] Z.-W. Lin, C. M. Ko, B.-A. Li, B. Zhang, and S. Pal, Phys. Rev. C **72**, 064901 (2005).

[41] B. I. Abelev *et al.* (STAR Collaboration), arXiv:0806.0513v1 (2008).

[42] PHOBOS [http://www.phobos.bnl.gov/Publications/Physics/Trig_Correl/index.htm].

[43] PHOBOS [http://www.phobos.bnl.gov/Publications/Physics/AA_2part_correl/index.htm].

[44] STAR, private communication [http://drupal.star.bnl.gov/STAR/publications/charge-independent-ci-and-charge-dependent-cd-correlations-function-centrality-formed-delta-phi-delta-eta-charged-p].

[45] B. Alver *et al.* (PHOBOS Collaboration), Phys. Rev. C **77**, 014906 (2008).

[46] B. Alver *et al.* (PHOBOS Collaboration), Phys. Rev. C **81**, 034915 (2010).

[47] B. Alver, M. Baker, C. Loizides, and P. Steinberg, arXiv:0805.4411v1 (2008).

[48] G. L. Ma *et al.*, Phys. Lett. B **641**, 362 (2006).

[49] G. L. Ma *et al.*, Eur. Phys. J. C **57**, 589 (2008).

[50] S. Zhang *et al.*, Phys. Rev. C **76**, 014904 (2007).

[51] W. Li *et al.*, Phys. Rev. C **80**, 064913 (2009).

[52] M. Gyulassy and X.-N. Wang, Comput. Phys. Commun. **83**, 307 (1994).

[53] B. I. Abelev *et al.* (STAR Collaboration), arXiv:0912.3977v2 (2009).